Analysis on steady-state characteristics of widely tunable SG-DBR laser with residual facet reflectivity model

Xiaoying He,[1,2] Yonglin Yu,[1,*] Dexiu Huang,[1] Shan Jiang,[1] Wen Liu,[1] and D. N. Wang[2]

[1]*Wuhan National Laboratory for Optoelectronics, Huazhong University of Science and Technology, Wuhan 430074, China*

[2]*Department of Electrical Engineering, The Hong Kong Polytechnic University, Hung Hom, Kowloon, Hong Kong*

**Corresponding author: yonglinyu@mail.hust.edu.cn*

Received November 21, 2008; revised May 25, 2009; accepted May 26, 2009; posted May 28, 2009 (Doc. ID 104393); published July 8, 2009

An efficient way to model the distributed Bragg reflector type of semiconductor devices with residual facet reflectivity is presented. Particularly, to improve the performance of such laser from two different ways of tuning—the differential or simultaneous tuning of two reflectors—the impacts of residual facet reflectivity on the sampled grating, and the static characteristics of such laser, including tuning behavior, output power, and side mode suppression ratio, are discussed. It revealed that the position of the facet relative to the gratings as well as their reflectivities are important parameters and should be carefully designed and fabricated to ensure good performance for such devices. © 2009 Optical Society of America

OCIS codes: 140.3600, 250.5960.

1. INTRODUCTION

Wavelength-agile, single-frequency monolithic laser diode, sampled grating distributed Bragg reflector (SG-DBR) lasers, have become potential sources for advanced optical communication networks and optics sensors. Especially, monolithic tunable lasers could cover wavelength ranges of several tens of nanometers by using sophisticated Vernier-effect tuning [1–4]. Because sampled grating (SG) reflectors create comblike reflection spectra, only a little current tuning is needed to obtain comparatively large wavelength jumps. Although Vernier-effect tuning represents an efficient way to fully exploit the tuning range of semiconductor lasers, it leaves the lasers susceptible to some unintended reflectivities. Such unintended reflectivities come from the front and rear facets of the laser chip [5] and can potentially change the comblike reflection spectra of reflectors, e.g., the SG reflector.

In this paper, the influence of facet reflections on SG reflectors, the tuning behavior, the side-mode suppression ratios (SMSRs), and the output power of monolithic tunable SG-DBR lasers are discussed, and a statistical analysis related to the one emitting a wavelength of 1546 nm with an important laser design parameter will be presented.

2. MODEL DESCRIPTION AND EQUATIONS

Taking the facet reflectivity into account, a theoretical numerical model needs to be developed to obtain high performance and reduce the fabrication cost of the tunable SG-DBR laser. The model proposed in this paper is based on the transmission line theory with multisection [6]. This enables assessment of active and passive components integrations, e.g., gain section, phase section, gratings, as well as absorptive sections. The configuration of the SG-DBR laser is depicted in Fig. 1. The cleavage positions of two facets relative to the gratings are important. The reason is that the facet with strong reflectivity and grating would come into being an invisible Fabry–Pérot (F–P) cavity, which is shown in Fig. 1 with cavity length L_R.

A. Transmission Line Theory for Multisection Device

The finite reflection coefficient may easily be included in this model if necessary. For simplicity, we will neglect possible reflections at the interfaces of the active sections and the grating section and set a reference plane at the interface between the active and the phase sections at $z=0$. Therefore, in the steady state, the optical field remains unchanged after a round trip along the entire laser cavity [7]. The oscillation condition can be expressed as

$$r_{\mathrm{SG1}}(\lambda,N_1)C_{\mathrm{out}}r_{\mathrm{SG2}}(\lambda,N_2)\exp\{-2jk_1(\lambda,N_3)l_3\}\times\exp\{-2jk_2(\lambda,N_4)l_4\}=1, \quad (1)$$

where r_{SG1} and r_{SG2} are the complex field reflectivities of the front and rear grating reflectors, C_{out} is the power coupling efficiency between the active and passive section waveguides, and the complex wavenumbers for the active and the passive phase sections are given by [7]

$$k_1(\lambda,N_3)=\frac{2\pi}{\lambda}n_3(\lambda,N_3)+\frac{1}{2}j(g(\lambda,N_3)-\alpha_3(N_3)), \quad (2)$$

$$k_2(\lambda,N_4)=\frac{2\pi}{\lambda}[n_0+\Delta n(\lambda,N_4)]-\frac{1}{2}j(\alpha_0+\Delta\alpha(\lambda,N_4)), \quad (3)$$

where c is the light velocity in vacuum, n_3 and α_3 are the refractive index and the internal absorption of the active

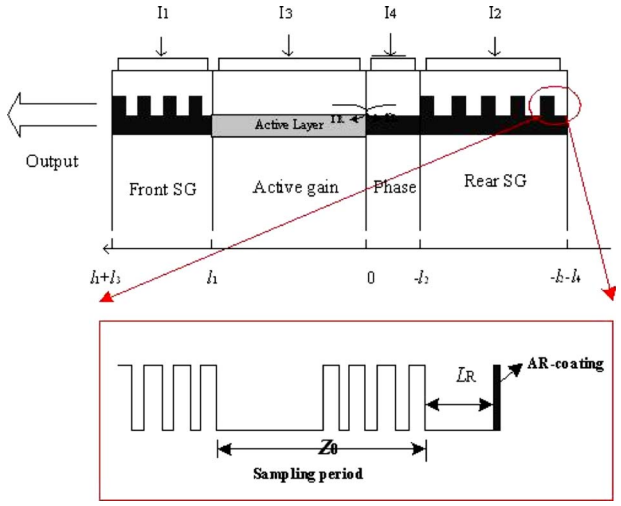

Fig. 1. (Color online) Schematic structure of tunable SG-DBR laser.

section, $g(\lambda,N_3)$ is the model gain of the active section, and n_0 and α_0 are the refractive index and the internal absorption of the passive phase section in the absence of carrier injection. N_3 and N_4 are the carrier densities of the active and the passive phase sections, respectively. The carrier-induced index and absorption changes are expressed as [8]

$$\Delta n(\lambda,N) = -\frac{e^2\lambda^2}{8\pi^2c^2n\varepsilon_0}\left(\frac{N_e}{m_e}+\frac{N_h}{m_h}\right), \tag{4}$$

$$\Delta\alpha(\lambda,N) = \frac{e^3\lambda^2}{4\pi^2c^3n\varepsilon_0}\left(\frac{N_e}{m_e\mu_e}+\frac{N_h}{m_h\mu_h}\right), \tag{5}$$

where ε_0 is the permittivity constant, and μ_e and μ_h are the mobilities of electrons and holes, respectively. N_e and N_h are the free electron and free hole concentrations, respectively, and n is the refractive index of the semiconductor. m_e and m_h denote the effective masses of the injected electrons and holes. The effective masses of the injected holes m_h can be expressed as [8]

$$m_h = \frac{m_{hh}^{3/2}+m_{lh}^{3/2}}{m_{hh}^{1/2}+m_{lh}^{1/2}}, \tag{6}$$

where n_1 and N_1 are, respectively, the mode refractive index and the carrier density of the front SG section. n_2 and N_2 are the mode refractive index and the carrier density of the rear SG section, respectively. The carrier densities N_1, N_2, and N_4 are determined by the injection currents I_1, I_2, and I_4 applied to the front SG grating, the rear SG grating, and the phase sections by

$$I_i = \eta_i e V_i R_i(N_i), \quad i=1,2,4, \tag{7}$$

where the spontaneous recombination rate per unit volume versus the carrier density is

$$R(N) = AN + BN^2 + CN^3. \tag{8}$$

Here e is the electron charge, V_1 and η_1 are the volume and the coupling coefficient of the effective injection current in the front SG section, V_2 and η_2 are the volume and the coupling coefficient of the effective injection current in the rear SG section, and V_4 and η_4 are the volume and the coupling coefficient of the effective injection current in the passive phase section. A, B, and C are recombination coefficients. A is the linear nonradiative recombination rate, B is the radiative recombination coefficient, and C is the Auger recombination coefficient.

From Eq. (1), the threshold gain and the phase condition can be described as

$$g_{\text{th}}(\lambda) = \alpha_3(\lambda,N_3) + \frac{l_4}{l_3}\alpha_0 + \frac{l_4}{l_3}\Delta\alpha(\lambda,N_4) + \frac{1}{l_3}\ln\left|\frac{1}{r_{\text{SG1}}(\lambda,N_1)r_{\text{SG2}}(\lambda,N_2)C_{\text{out}}}\right|, \tag{9}$$

$$h(\lambda) = \frac{4\pi n_3 l_3}{\lambda} + \frac{4\pi(n_0+\Delta n(\lambda,N_4))l_4}{\lambda} - \arg\{r_{\text{SG1}}(\lambda,N_1)r_{\text{SG2}}(\lambda,N_2)\} = 2\pi. \tag{10}$$

The full phase oscillation condition is solved to yield the longitudinal mode spectrum. The h function related to the phase oscillation condition is used for analyzing the stability properties and selecting the longitudinal modes. Due to the longitudinal modes for the SG-DBR laser, the lowest loss of each longitudinal mode is calculated based on Eq. (9), which can be written as

$$\alpha_m(\lambda_m) = \alpha_3(\lambda_m,N_3) + \frac{l_4}{l_3}\alpha_0 + \frac{l_4}{l_3}\Delta\alpha(\lambda_m,N_4) + \frac{1}{l_3}\ln\left|\frac{1}{r_{\text{SG1}}(\lambda_m,N_1)r_{\text{SG2}}(\lambda_m,N_2)C_{\text{out}}}\right|, \tag{11}$$

where m is the number of distinct longitudinal modes. Unlike a conventional F–P laser, the SG-DBR laser has different longitudinal mode losses due to the front and the rear SG reflectors.

B. Sampled Grating Section with Facet Reflectivity

The idea of SG relies on periodical modulation (sampling) of the grating such that zones of the grating are periodically removed. To derive the transfer matrix [9] for the sampled reflector, we need to consequently multiply the transfer matrices corresponding to the corrugation periods with the matrices corresponding to the propagation in the homogeneous waveguide regions. The transfer matrix for one corrugation period in the kth subsection of grating regions is $F_B(\lambda)$, which can be written as follows [10]:

$$F_B^{(k)}(\lambda) = \begin{bmatrix} \frac{n_{3g}+n_{4g}}{2\sqrt{n_{3g}n_{4g}}} & \frac{n_{3g}-n_{4g}}{2\sqrt{n_{3g}n_{4g}}} \\ \frac{n_{3g}-n_{4g}}{2\sqrt{n_{3g}n_{4g}}} & \frac{n_{3g}+n_{4g}}{2\sqrt{n_{3g}n_{4g}}} \end{bmatrix} \begin{bmatrix} e^{j\beta\Lambda/2} & 0 \\ 0 & e^{-j\beta\Lambda/2} \end{bmatrix} \times \begin{bmatrix} \frac{n_{4g}+n_{3g}}{2\sqrt{n_{3g}n_{4g}}} & \frac{n_{4g}-n_{3g}}{2\sqrt{n_{3g}n_{4g}}} \\ \frac{n_{4g}-n_{3g}}{2\sqrt{n_{3g}n_{4g}}} & \frac{n_{4g}+n_{3g}}{2\sqrt{n_{3g}n_{4g}}} \end{bmatrix} \begin{bmatrix} e^{j\beta\Lambda/2} & 0 \\ 0 & e^{-j\beta\Lambda/2} \end{bmatrix}. \tag{12}$$

The transmission matrix of the uncorrugated space in the kth subsection can be expressed as [10]

$$F_S^{(k)}(\lambda) = \begin{bmatrix} e^{j\beta L_s} & 0 \\ 0 & e^{-j\beta L_s} \end{bmatrix}, \tag{13}$$

and the transmission matrix in the invisible F–P cavity can be written as

$$F_R(\lambda) = \begin{bmatrix} e^{j\beta L_R} & 0 \\ 0 & e^{-j\beta L_R} \end{bmatrix}, \tag{14}$$

where β is the propagation constant, Λ is the grating pitch, and n_{eff} is the effective refractive index of the SG sections. L_s is the uncorrugated space length in a sampling period. L_R is the distance of the facet relative to the gratings. n_{3g} and n_{4g} are refractive indices of refractive index step of a corrugation period, respectively. All these refractive indices are related to injection carrier densities of reflectors.

The transfer matrix of the output facet [right antireflectivity (AR) coating facet] can be expressed as

$$T_R = \frac{1}{1-R_R}\begin{bmatrix} e^{-j\phi_r/2} & -R_R e^{j\phi_r/2} \\ -R_R e^{-j\phi_r/2} & e^{j\phi_r/2} \end{bmatrix}, \tag{15}$$

and the transfer matrix of the rear facet (left AR-coating facet) can be expressed as

$$T_L = \frac{1}{1-R_L}\begin{bmatrix} e^{-j\phi_l/2} & R_L e^{-j\phi_l/2} \\ R_l e^{j\phi_l/2} & e^{j\phi_l/2} \end{bmatrix}, \tag{16}$$

where both R_R and R_L can be set as 0. The transfer matrix of the rear SG reflectors with facet reflectivity can be expressed as

$$M_{\text{SG2}} = [[F_s][F_B]^n]^N[F_R][T_L], \tag{17}$$

where n is the Bragg period number of the rear SG reflector. N is the sampling period of two gratings. The transfer matrix of the front SG reflector is similar to Eq. (17).

C. Material Gain and Rate Equation

The material gain coefficient is given by

$$G_m = a(N - N_0) - b(\lambda - \lambda_p)^2, \tag{18}$$

where a is the differential gain and b is a gain constant. Of interest here is the wavelength tuning obtained by changing currents of two SG grating sections. Since a four-electrode distributed Bragg reflector (DBR) laser can be regarded as a F–P laser, multimode rate equations can be used to describe the steady-state behaviors ($m = 1,2,\ldots$, corresponding to longitudinal modes) [11–13],

$$\frac{dS_m(t)}{dt} = \frac{c}{n_r}\Gamma g_m(N_3,\lambda_m)S_m(t) - \frac{c}{n_r}\alpha_m(\lambda_m,N_1,N_2,N_3,N_4)S_m(t) + \frac{\Gamma \gamma K_m N(t)}{\tau_{\text{sp}}}, \tag{19}$$

$$\frac{dN_3(t)}{dt} = \frac{I_3}{eV_3} - R_3(N_3(t)) - \frac{c}{n_r}\left[\sum_m g(N_3,\lambda_m)S_m(t)\right], \tag{20}$$

$$\frac{dN_i(t)}{dt} = \frac{I_i(t)}{eV_i} - R_i(N_i(t)), \quad i = 1,2,4, \tag{21}$$

where the gain g and the mode loss α_m have been given in Eqs. (18) and (11), respectively. S_m is the photon density of the mth longitudinal mode with the wavelength λ_m. n_r is the effective refractive index in the active section; I_3 and I_4 are, respectively, the currents applied to the active and phase control sections; and Γ is the optical confinement factor.

3. STEADY-STATE THEORETICAL RESULTS WITH LOW FACET REFLECTIVITY

In our theoretical model of the SG-DBR lasers, the facet reflectivities have been considered. The material and the geometrical parameters about the SG-DBR laser are given in Table 1, and the currents about the active and phase sections, respectively, would be biased at 150 and 0 mA.

The tuning characteristics of a SG-DBR laser are essential features for verifying the accuracy of our theoretical model, which are shown in Fig. 2 by tuning the currents of the two SG reflectors from 0 to 10 mA. Two facet reflectivities and the distance of zero between the facet and the grating of 10^{-5} are used in Figs. 2–5. In Fig. 2, the full tuning range of the device is ~1530 to 1570 nm, which is more than sufficient to span the whole of the C band. Nine supermodes are demonstrated with nine different colors, where the alignment of the front and rear reflectivity peaks was switched from one pair to another. The map of every supermode can be divided into several saddle points, and the small side steps indicate borderlines of every saddle point and the boundaries of the longitudinal cavity modes, which are related to cavity-mode hops. The emission wavelength can be operated continuously within one cavity mode, where the cavity mode shifts within overlapped reflection peaks of two SG reflectors. Although the tuning characteristics presented by our simulation are basically in agreement with experimental results reported in the literature, any imperfections of the SG-DBR fabrication, such as waveguide thickness deviations, overgrowth imperfections, etc., are difficult to account for in the theoretical simulation.

Based on the tuning characteristics, the maximal SMSR would occur at the points where a peak of each reflector is exactly aligned with the same cavity mode, i.e., in the center of the grids with a high SMSR of Fig. 3, where the SMSR contour map is illustrated. The SMSR contour map is divided into many saddle regions. Serious deterioration of the SMSR has happened in two regions. One region is the high front and the low rear reflector currents, and the other is the high rear and the low front reflector currents. At the boundary of supermodes jumping, the SMSR appears disorderly and unstable due to the nonuniform reflectivity spectrum envelope of the SG. The calculated output power map of the SG-DBR laser is shown in Fig. 4 as a function of both reflector currents, where saddle points are observed at certain locations: a maximum with respect to the front SG reflector current

Table 1. Parameters of the SG-DBR Laser [5–9]

Parameter	Symbol	Value
Active section:		
Thickness of active layer	d	0.15 μm
Width of active layer	w	1.2 μm
Length of active section	l_3	500 μm
Confinement factor	Γ	0.32
Mode refractive index	n_3	3.245
Nonradiative recombination coefficient	A	1.5×10^{8} s^{-1}
Bimolecular recombination coefficient	B	4×10^{-16} m^3 s^{-1}
Auger recombination coefficient	C	5×10^{-41} m^6 s^{-1}
Central wavelength	λ_p	1.550 μm
Internal absorption loss	α	2100 m^{-1}
Spontaneous emission factor	γ	10^{-4}
Spontaneous electron lifetime	τ_{sp}	3 ns
Differential gain	a	2.5×10^{-16} cm^{-2}
Gain constant	b	0.23 nm^{-2}
Passive phase section:		
Thickness of waveguide layer	d	0.38 μm
Width of waveguide layer	W	1.2 μm
Length of waveguide section	l_4	50 μm
Confinement factor	Γ	0.4
Mode refractive index	n_4	3.21
Nonradiative recombination coefficient	A	1.68×10^{8} s^{-1}
Bimolecular recombination coefficient	B	2.8×10^{-17} m^3 s^{-1}
Auger recombination coefficient	C	5.24×10^{-42} m^6 s^{-1}
Facet field reflectivity	r_2	0.4–0.000 01
Internal absorption loss without injection current	α	1200 m^{-1}
Injection efficiency	η_{in}	0.7
SG:		
Thickness of waveguide layer	d	0.38 μm
Width of waveguide layer	w	1.2 μm
Nonradiative recombination coefficient	A	2.5×10^{8} s^{-1}
Bimolecular recombination coefficient	B	1×10^{-17} m^3 s^{-1}
Auger recombination coefficient	C	4×10^{-41} m^6 s^{-1}
Confinement factor	Γ	0.35
Effective refractive index	n_{SG}	3.4
Internal absorption loss without injection current	α	1200 m^{-1}
Variation in refractive index	δn_{eff}	6×10^{-3}
Injection efficiency	η_{in}	0.85
Length of the front SG section	l_1	360 μm
Length of the rear SG section	l_2	600 μm

coincides with a maximum with respect to the rear SG reflector current. The increase with current of the absorption losses in two SG reflectors causes the saddle point to shift toward the boundary of modes hopping, in which it has a large current in the rear reflector and a small current in the front reflector. However, for high currents, the saddle point even disappears. Therefore, the absorption loss of the front reflector has a larger effect on the output power than that of the rear, especially for a long front section, since the output light has to pass through this section.

A sample of high spectral purity about the laser is illustrated in Fig. 5, showing simulated optical emission

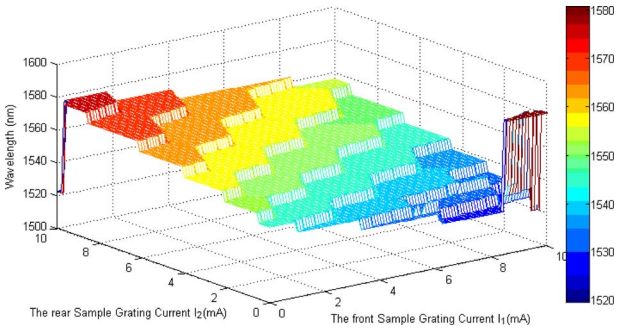

Fig. 2. (Color online) Wavelength tuning versus currents of two SG reflector sections.

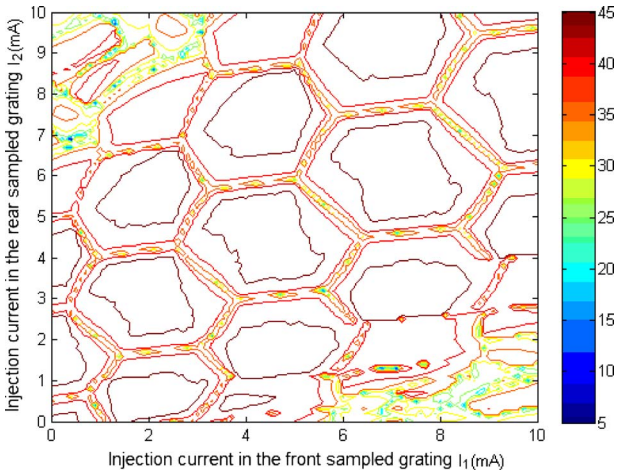

Fig. 3. (Color online) SMSR map versus currents of the front and the rear SG reflector sections.

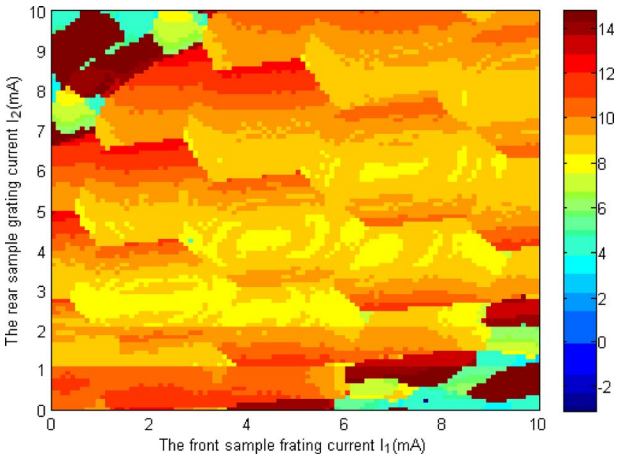

Fig. 4. (Color online) Output power map versus currents of the front and the rear SG reflector sections.

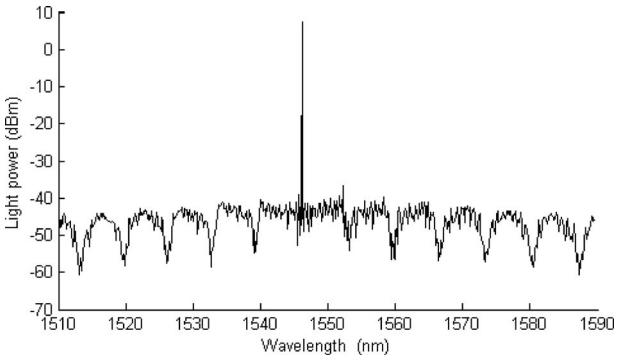

Fig. 5. Emission spectrum of the SG-DBR laser at a wavelength of 1576.59 nm.

spectrum of the best supermode of 1576.59 nm. The output power will reach 10 dBm with a high SMSR of 40 dB.

4. INFLUENCES OF FACET REFLECTIVITY ON SG-DBR LASER

Such reflections, for example, mainly arise from the front and rear facets of the laser chip. Typically, at least AR-coating facets are needed to emphasize the reflection spectrum of the distributed SG reflectors. Not only SG reflectors, but the Vernier-effect tuning also is susceptible to the facet reflections.

There are two tuning ways (differential and simultaneous tuning) to be deployed in this laser. Differential tuning is used to shift the wavelength by tuning only one reflector and leaving the other one unchanged. Nevertheless, the simultaneous tuning is done by simultaneous tuning of both reflectors. Computation of the behaviors of emission wavelength, output power, and SMSR during differential and simultaneous tuning is sufficient to characterize the laser.

A. Influences of Facet Reflectivity on the Sampled Grating

Now, we start discussing the effect of facet reflectivity on the reflection spectrum of the rear SG, which is illustrated in Fig. 6. Figure 6(a) shows the reflection spectrum of the rear reflector in the practically unperturbed situation about facet reflection ($R_2=10^{-5}$), and Figs. 6(b) and 6(c) show the reflection spectrum of the rear reflector in the presence of strong facet reflection ($R_2=0.1$).

The reflection spectrum becomes substantially impaired by the strong facet reflections. In Fig. 6(b), some reflection peaks are suppressed, while others are enhanced. Furthermore, the sidelobes between reflection peaks can be substantially enhanced and distorted. The reason is that an invisible F–P cavity between the facet coating and the grating interferes with the SG reflection spectrum. That is to say, the influence of the facet reflections is determined by the position of the facet relative to the gratings, denoted as distance L_R. For example as shown in Fig. 6(b), L_R is chosen to be 23 μm, which results in the free spectrum width of 15.3 nm of the invisible F–P cavity. However, the reflection peak spacing of the grating is close to 7.8 nm. Thus the amplitude of reflection peaks appears to have interleaving variation, i.e., the one peak is enhanced and the adjacent peak is suppressed. In Fig. 6(c), the strong facet reflectivity leads to the peak reflectivities with long wavelengths decreasing and bifurcating and makes the sidelobes around every peak enhanced. That is because without F–P cavity length ($L_R=0$ μm) the strong facet reflectivity would directly enhance the whole reflection spectrum of the SG including the sidelobes.

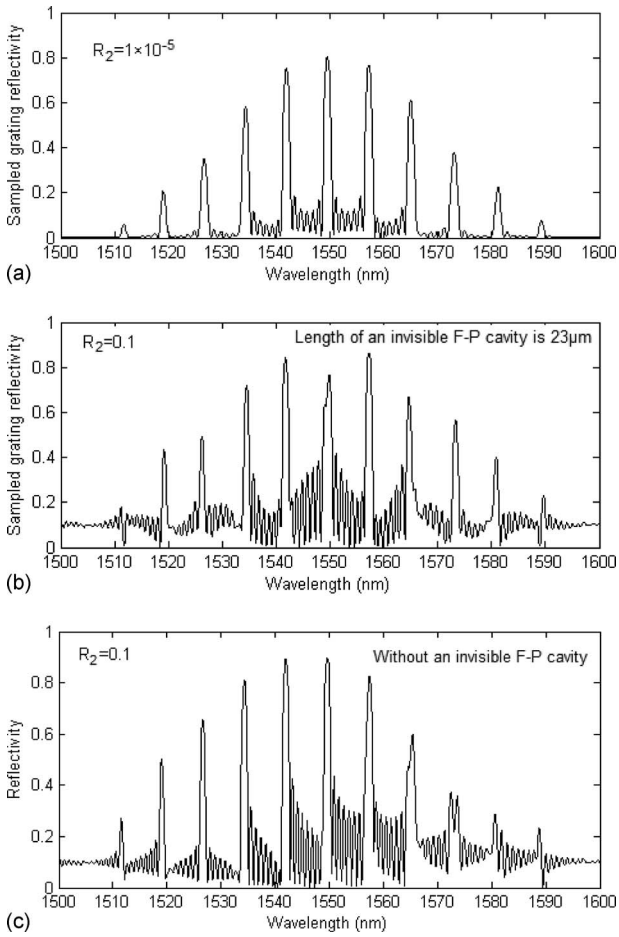

Fig. 6. SG reflection spectra illustrating distortion effects owing to facet reflections.

B. Influences of Facet Reflectivity on the SG-DBR Laser by Difference Tuning

To merely consider the influences of facet reflectivity on the laser, the invisible cavity length L_R is set as 0 μm. Using this static model for numerical simulation, the transition of tuning behavior and output power between the weak and strong facet mirror reflectivities is shown in Fig. 7. In the presence of only two weak facet reflections ($R_1=1\times10^{-5}$,$R_2=1\times10^{-5}$) of Fig. 7(a), the current tuning in the rear SG section can result in large wavelength jumps, so-called supermode hops, whose interval is following the spacing of reflection peaks about SG. At a moderate facet reflection ($R_1=1\times10^{-3}$,$R_2=1\times10^{-3}$), shown in Fig. 7(b), the tuning behavior and the output power variation are almost identical with that of the SG-DBR laser with weak facet mirror reflectivity ($R_1=1\times10^{-5}$,$R_2=1\times10^{-5}$). Nevertheless, at a high facet reflection ($R_1=1\times10^{-1}$,$R_2=1\times10^{-1}$), at the high injection current of 10 mA, a supermode hop appears. That is because the en-

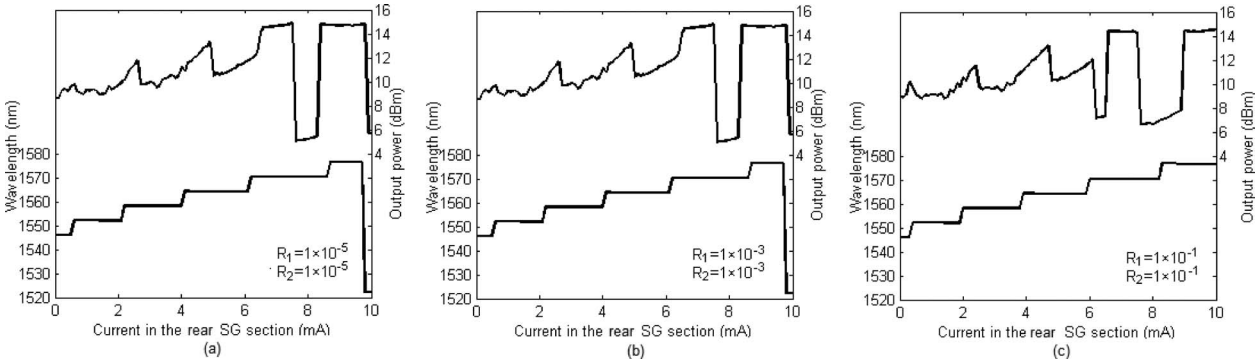

Fig. 7. Tuning characteristics and output power of tunable lasers at three different front and rear facet reflectivities.

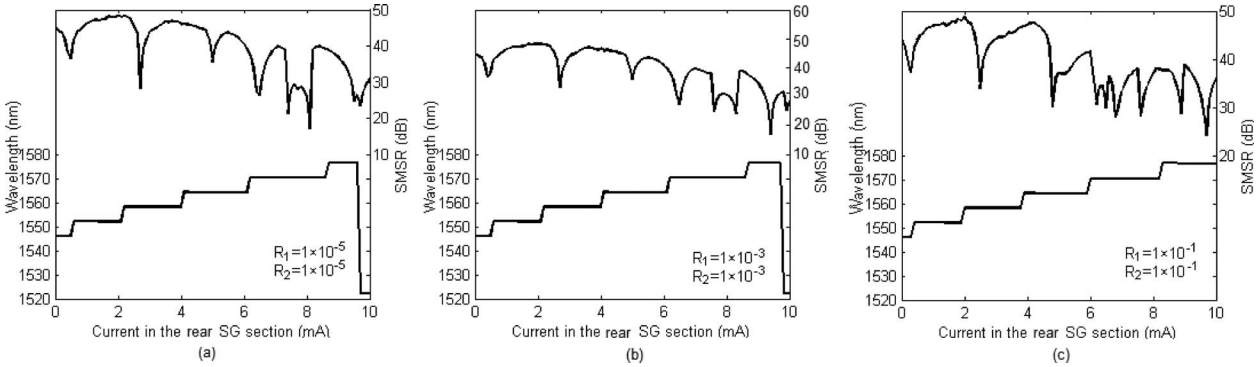

Fig. 8. Tuning characteristics and SMSR of tunable lasers at three different front and rear facet reflectivities.

hanced or suppressed reflection peak can make another mode within the peak take part in mode competition. From Fig. 7, with the increase in facet mirror reflectivity, the output power has a large variation at the high rear DBR current.

The SMSR during differential tuning is illustrated in Fig. 8. With the increase in rear DBR current, the maximal SMSR at each tuning step is decreasing. The SMSR appears with a large variation at high rear DBR current, especially with a high facet reflection ($R_1=1\times10^{-1}$,$R_2=1\times10^{-1}$).

C. Influences of Facet Reflectivity on the SG-DBR Laser by Simultaneous Tuning

The tuning behaviors, the output power, and the SMSR during simultaneous tuning are shown in Figs. 9–11, respectively. From Fig. 9, when the reflectivities of the two facets are not over 10^{-3}, the wavelength tuning behaviors still conform to the tuning rule of the Vernier effect. When the injection current is tuned from 0 to 10 mA, it is shown in Figs. 9(a) and 9(b) that by simultaneous tuning three supermode hops have been illustrated. As shown in the second supermode, three cavity modes have been obtained by following the increase in the injection current. At the high facet reflectivity of 10^{-1}, the tuning behaviors become irregular. With high facet reflectivity, some unpredictable modes are taken into the mode competition, especially the unpredictable cavity modes, which break the simultaneous tuning rule about cavity modes. In the presence of weak and moderate facet reflectivities, the variation range is 3 dB. At high facet reflectivity, the vitiation range increases to 3.4 dB.

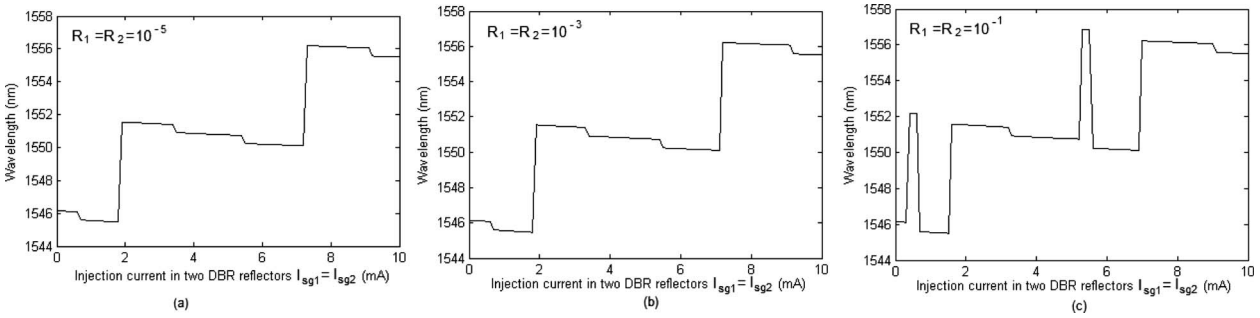

Fig. 9. Tuning behaviors as a function of two facet reflectivities for different device designs.

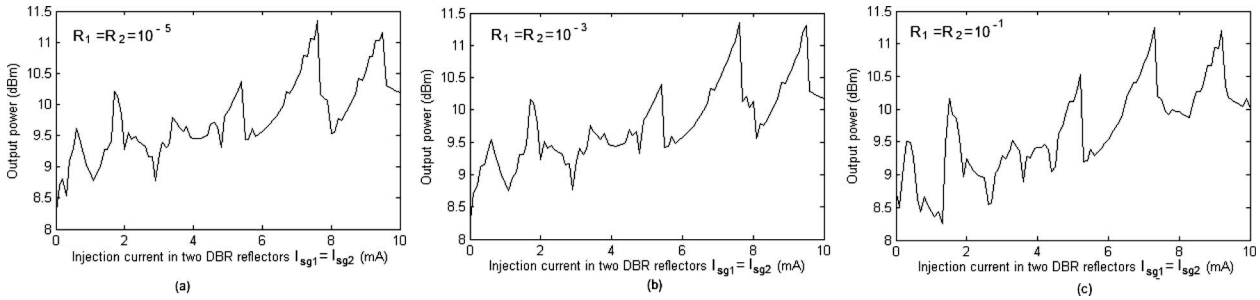

Fig. 10. Output power as a function of two facet reflectivities for different device designs.

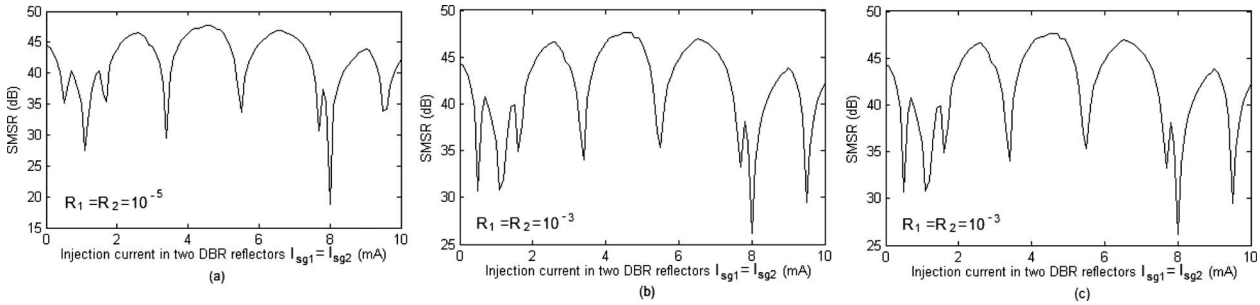

Fig. 11. SMSR as a function of two facet reflectivities for different device designs.

In Fig. 11, the good SMSR has been displayed at weak and moderate facet reflectivities. However, the irregular mode jumping can lead to the SMSR curve change.

D. Influences of Facet Reflectivity on SG-DBR with Different Grating Reflectivities

To further assess the level of influence that is caused by the facet reflections, we theoretically make statistical analyses on the emitting wavelength, the output power, and the SMSR at an emitting wavelength of 1546 nm with different facet reflectivities, which are shown in Fig. 12. Using our given device model, the power reflectivity of both facets synchronously varies from 10^{-1} to 10^{-5}, and the currents of two SG reflector sections and that of the phase section are all specified at 0 mA.

The dc refractive index change mainly affects the reflectivity value of the SG reflector. It is illustrated in Fig. 12 that a smaller dc refractive index change that results in the SG-DBR laser round the emitting wavelength of 1546 nm has high output power and excellent SMSR, while a high dc refractive index is beneficial for suppressing the impact of facet reflectivity on the output power and the SMSR. The tolerance on facet reflectivity is determined by the dc refractive index: high dc refractive index can decrease the variation in output power, SMSR, as well as redshift about emitting wavelength. However, too high of a dc reflective index change on SG may cause spatial hole burning, which has not been taken into account in our model analysis. From Fig. 12(a), as the reflectivity of two facets increases, the emitting wavelength presents a redshift phenomenon, which is corresponding to additional resonance of an invisible F–P cavity formed by the ended grating and facet coating with high reflectivity. At the dc refractive index of low to 12×10^{-3}, when the facet reflectivity is over 10^{-3}, the variation in the output power, the decrease in the SMSR, and the emitting wavelength shift are all presented.

The reflection peak around the Bragg wavelength has the highest reflectivity in the SG. Thus, the phenomenon at this emitting point would deduce to the impact of the facet reflectivity on the steady-state characteristics of the SG-DBR laser over the whole tuning range.

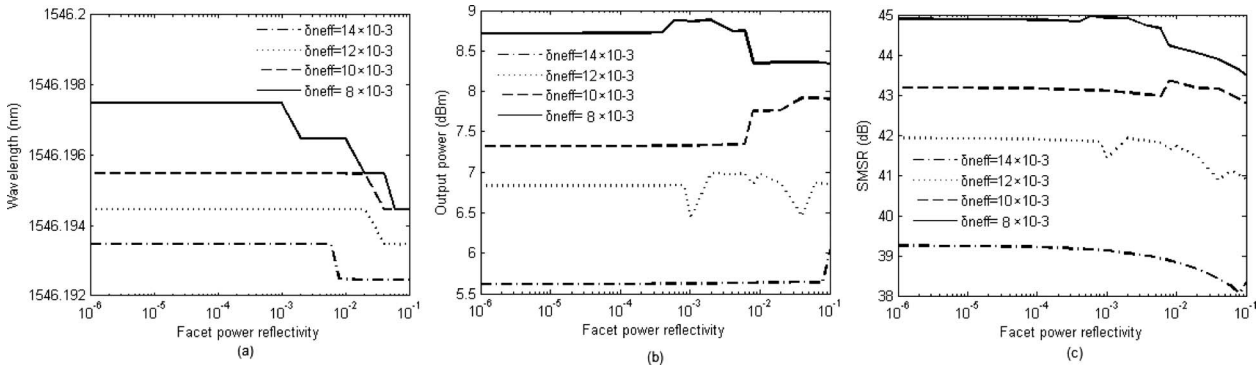

Fig. 12. Tuning behaviors, output power, and SMSR as functions of two facet reflectivities for different device designs.

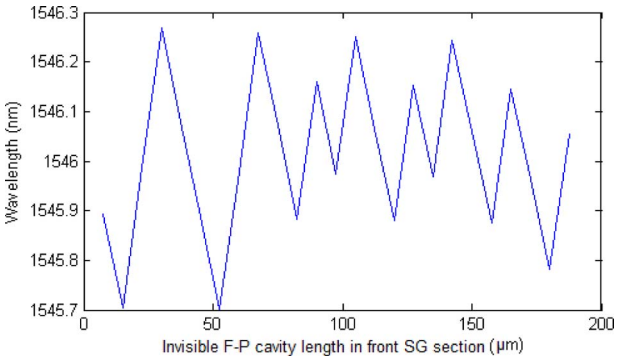

Fig. 13. (Color online) Wavelength variation versus the invisible F–P cavity length change.

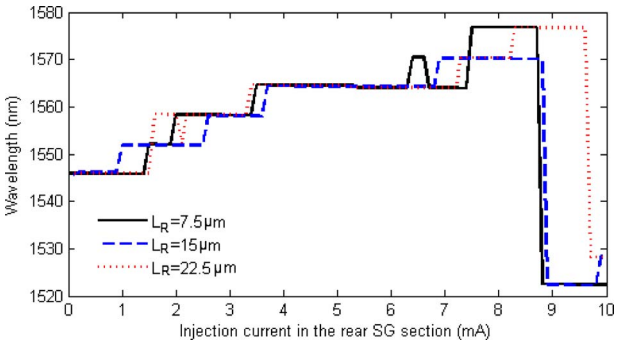

Fig. 14. (Color online) Tuning behaviors as a function of the rear section for L_R values.

E. Influences of Invisible Fabry–Pérot Cavity Length on SG-DBR

For discussing the influences of the invisible F–P cavity length, we change the invisible F–P cavity length discretely to observe emitting wavelength in Fig. 13, where all injection currents in the SG-DBR laser are fixed (I_1 =0 mA,I_2=0 mA,I_3=150 mA,I_4=0 mA). With the increase in the invisible F–P cavity length, the emitting wavelength varies around 1546 nm over 0.6 nm. It is shown that the invisible F–P cavity length would indirectly influence the F–P modes. Figure 14 shows that the L_R lengths influence the tuning behaviors. The L_R length can influence cavity modes, as well as supermodes. Therefore, the L_R length could break the Vernier effect.

5. CONCLUSION

A theoretical model of the tunable SG-DBR laser for considering the residual facet reflectivity has been proposed. The steady-state characteristics have been simulated and analyzed. Furthermore, the impacts of residual facet reflectivity on SG and static characteristics of such laser, including the tuning behavior, the output power, and the SMSR, have been discussed. The impact of residual facet reflectivity mainly lies on the position of the facet relative to the gratings. High residual facet reflectivities could lead to irregular tuning behavior, amplitude variation on the output power, and the side-mode supression ratio (SMSR). Moderately high dc refractive index is beneficial for suppressing the impact of facet reflectivity on the output power and the SMSR. However, a low dc refractive index could boost the output power and the SMSR at the emitting wavelengths. Moreover, a statistical analysis on steady-state characteristics has been presented, which revealed that facet reflectivities of the order of 10^{-3}–10^{-4} or below are required to achieve a SG-DBR laser with good performance. The invisible F–P cavity length has a considerable influence on the whole tuning behavior of the SG-DBR laser.

ACKNOWLEDGMENTS

The authors undertook this work with the support of the National Natural Science Foundation of China (NSFC) under grant 60677024, the National High Technology Research Development Program of China under grant 2006AA03Z0427, and The Hong Kong Polytechnic University research grants A-PH82 and G-U501.

REFERENCES

1. J. Buus and E. J. Murphy, "Tunable lasers in optical networks," J. Lightwave Technol. **24**, 5–11 (2006).
2. L. A. Coldren, G. A. Fish, Y. Akulova, J. S. Barton, and C. W. Coldren, "Tunable semiconductor lasers: a tutorial," IEEE J. Lightwave Technol. **22**, 193–202 (2004).
3. G. Sarlet, G. Morthier, and R. Baets, "Control of widely tunable SSG-DBR lasers for dense wavelength division multiplexing," IEEE J. Lightwave Technol. **18**, 1128–1138 (2000).
4. L. Ponnampalam, N. D. Whitbread, R. Barlow, G. Busico, A. J. Ward, J. P. Duck, and D. J. Robbins, "Dynamically controlled channel-to-channel switching in a full-band DS-DBR laser," J. Quantum Electron. **42**, 223–231 (2006).
5. A. Tsigopoulos, T. Sphicopoulos, I. Orfanos, and S. Pantelis, "Wavelength tuning analysis and spectral characteristics of three-section DBR lasers," IEEE J. Quantum Electron. **28**, 415–426 (1992).
6. B. Tromborg, H. Olesen, X. Pan, and S. Saito, "Transmission line description of optical feedback and injection locking for Fabry–Perot and DFB lasers," IEEE J. Quantum Electron. **23**, 1875–1889 (1987).
7. X. Pan, H. Olesen, and B. Tromberg, "A theoretical model of multielectrode DBR lasers," IEEE J. Quantum Electron. **24**, 2423–2432 (1988).
8. R. A. Soref and J. Larenzo, "All-silicon active and passive guided-wave components for λ=1.3 and 1.6 μm," IEEE J. Quantum Electron. **22**, 873–879 (1986).
9. M. G. Davis and R. F. O'Dowd, "A transfer matrix method based large signal dynamic model for multielectrode DFB lasers," IEEE J. Quantum Electron. **30**, 2458–2466 (1994).
10. O. A. Lavrova and D. J. Blumenthal, "Detailed transfer matrix method-based dynamic model for multisecion widely tunable GCSR lasers," J. Lightwave Technol. **18**, 1274–1376 (2000).
11. G. P. Agrawal, *Long-Wavelength Semiconductor Lasers* (Van Nostrand Reinhold, 1986).
12. D. Marcuse, "Computer simulation of laser photon fluctuations: theory of single-cavity laser," IEEE J. Quantum Electron. **20**, 1139–1148 (1984).
13. D. Marcuse, "Computer simulation of laser photon flucturations: DFB lasers," IEEE J. Quantum Electron. **21**, 161–167 (1985).